Fundamental limits on the rate of bacterial cell division

Nathan M. Belliveau[†, 1]**, Griffin Chure**[†, 2, 3]**, Christina L. Hueschen**[4]**, Hernan G. Garcia**[5]**, Jané Kondev**[6]**, Daniel S. Fisher**[7]**, Julie Theriot**[1, 8]**, Rob Phillips**[1, 2, 9, *]

*For correspondence:

[†]These authors contributed equally to this work

[1]Department of Biology, University of Washington, Seattle, WA, USA; [2]Division of Biology and Biological Engineering, California Institute of Technology, Pasadena, CA, USA; [3]Department of Applied Physics, California Institute of Technology, Pasadena, CA, USA; [4]Department of Chemical Engineering, Stanford University, Stanford, CA, USA; [5]Department of Molecular Cell Biology and Department of Physics, University of California Berkeley, Berkeley, CA, USA; [6]Department of Physics, Brandeis University, Waltham, MA, USA; [7]Department of Applied Physics, Stanford University, Stanford, CA, USA; [8]Allen Institute for Cell Science, Seattle, WA, USA; [9]Department of Physics, California Institute of Technology, Pasadena, CA, USA; [*]Contributed equally
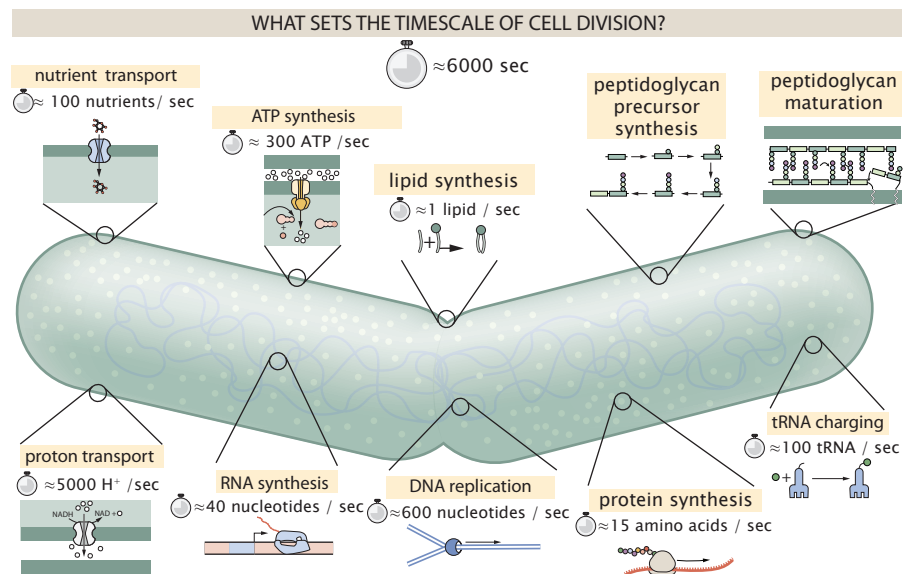

Abstract

Introduction

The range of bacterial growth rates can be enormous. In natural environments, some microbial organisms might double only once per year, whereas in comfortable laboratory conditions growth can be rapid with several divisions per hour. This remarkable diversity illustrates the intimate relationship between environmental conditions and the rates at which cells convert nutrients into new cellular material. This relationship between the environment and cellular growth rate has remained a major topic of inquiry in bacterial physiology for over a century (*Jun et al., 2018*). In 1958, Schaecter, Malløe, and Kjeldgaard reported the discovery of a logarithmic relationship between the total cellular protein content and the cellular growth rate, revealing a fundamental relationship between the environment and the composition of the intracellular milieu (*Schaechter et al., 1958*).

Over the past decade, a remarkable body of work has reexamined this relationship with single-cell and single-protein resolution using modern methods of video microscopy (*Si et al., 2017*; *Harris and Theriot, 2018*) and through advances in mass spectrometry and sequencing technologies (*Schmidt et al., 2016*; *Li et al., 2014*). This has permitted quantitative insight into how bacteria like *E. coli* allocate their cellular resources under nutrient-limitation, and following genomic and pharmacological perturbations (*Scott et al., 2010*; *Hui et al., 2015*; *Basan et al., 2015*). This body of experimental data places us in the auspicious position to explore how the abundance of essential protein complexes are related to the growth rate of the population and interrogate what biological processes may set the speed limit of bacterial growth.

In this work, we seek to leverage a collection of proteomic data sets of *Escherichia coli* across 31 growth conditions (*Valgepea et al., 2013*; *Li et al., 2014*; *Peebo et al., 2015*; *Hui et al., 2015*; *Schmidt et al., 2016*) to quantitatively explore what biological processes may set the speed limit of bacterial growth. Broadly speaking, we entertain several classes of hypotheses as are illustrated in *Figure 1*. First, we consider potential limits on the transport of nutrients into the cell. We address this hypothesis by performing an order-of-magnitude estimate for how many carbon atoms needed

WHAT SETS THE TIMESCALE OF CELL DIVISION?

≈6000 sec

nutrient transport
≈ 100 nutrients / sec

ATP synthesis
≈ 300 ATP /sec

lipid synthesis
≈1 lipid / sec

peptidoglycan precursor synthesis

peptidoglycan maturation

proton transport
≈5000 H⁺ /sec

RNA synthesis
≈40 nucleotides / sec

DNA replication
≈600 nucleotides / sec

protein synthesis
≈15 amino acids / sec

tRNA charging
≈100 tRNA / sec

Figure 1. Transport and synthesis processes necessary for cell division. We consider an array of processes necessary for a cell to double its molecular components. Such processes include the transport of carbon across the cell membrane, the production of ATP, and fundamental processes of the central dogma namely RNA, DNA, and protein synthesis. A schematic of each synthetic or transport category is shown with an estimate of the rate per macromolecular complex. In this work, we consider a standard bacterial division time of ≈ 6000 sec.

42 to facilitate this requirement given a 6000 second division time. As a second hypothesis, we consider
43 the possibility that there exists a fundamental limit on how quickly the cell can generate ATP. We
44 approach this hypothesis from two angles, considering how many ATP synthase complexes must be
45 needed to churn out enough ATP to power protein translation followed by an estimation of how
46 many electron transport complexes must be present to maintain the proton motive force. Our third
47 and final class of hypotheses centers on the synthesis of a variety of biomolecules. Our focus is
48 primarily on the stages of the central dogma as we estimate the number of protein complexes
49 needed for DNA replication, transcription, and protein translation.

50 With estimates in hand for each of these processes, we turn to our collection of data sets to
51 assess the accuracy of our estimates. In broad terms, we find that the majority of our estimates are
52 in line with experimental observations, with protein copy numbers apparently well-tuned for the
53 task of cell doubling. This allows us to systematically scratch off the hypotheses diagrammed in
54 *Figure 1* as setting possible speed limits. Ultimately, we find that protein translation (particularly the
55 generation of new ribosomes) acts as 1) a rate limiting step for the *fastest* bacterial division, and 2)
56 the major determinant of bacterial growth across all nutrient conditions we have considered under
57 steady state, exponential growth. This perspective is in line with the linear correlation observed
58 between growth rate and ribosomal content (usually quantified through the ratio of RNA to protein)
59 for fast growing cells (*Scott et al., 2010*), but suggests a more prominent role for ribosomes in
60 setting the doubling time across all conditions of nutrient limitation. Here we again leverage the
61 quantitative nature of this data set and present a quantitative model of the relationship between
62 the fraction of the proteome devoted to ribosomes and the speed limit of translation, revealing
63 a fundamental tradeoff between the translation capacity of the ribosome pool and the maximal
64 growth rate.

Nutrient Transport

66 In order to build new cellular mass, the molecular and elemental building blocks must be scavenged
67 from the environment in different forms. Carbon, for example, is acquired via the transport of
68 carbohydrates and sugar alcohols with some carbon sources receiving preferential treatment

69 in their consumption (*Monod, 1947*). Phosphorus, sulfur, and nitrogen, on the other hand, are
70 harvested primarily in the forms of inorganic salts, namely phosphate, sulfate, and ammonia
71 (*Jun et al., 2018*; *Assentoft et al., 2016*; *Stasi et al., 2019*; *Antonenko et al., 1997*; *Rosenberg et al.,*
72 *1977*; *Willsky et al., 1973*). All of these compounds have different permeabilities across the cell
73 membrane and most require some energetic investment either via ATP hydrolysis or through the
74 proton electrochemical gradient to bring the material across the hydrophobic cell membrane. Given
75 the diversity of biological transport mechanisms and the vast number of inputs needed to build a
76 cell, we begin by considering transport of elemental requirements as a possible rate-limiting step of
77 bacterial cell division.

78 The elemental composition of *E. coli* has received much quantitative attention over the past
79 half century (*Neidhardt et al., 1991*; *Taymaz-Nikerel et al., 2010*; *Heldal et al., 1985*; *Bauer and Ziv,*
80 *1976*), providing us with a starting point for estimating the copy numbers of various transporters.
81 While there is some variability in the exact elemental percentages (with different uncertainties), we
82 can estimate that the dry mass of a typical *E. coli* cell is $\approx$ 45% carbon (BNID: 100649, *Milo et al.*
83 (*2010*)), $\approx$ 15% nitrogen (BNID: 106666, *Milo et al.* (*2010*)), $\approx$ 3% phosphorus (BNID: 100653, *Milo*
84 *et al.* (*2010*)), and 1% sulfur (BNID: 100655, *Milo et al.* (*2010*)). In the coming paragraphs, we will
85 examine how many transporters and/or channels must be present to maintain these elemental
86 compositions with a moderate doubling time of 6,000 s.

Carbon Transport

88 We begin with the most abundant element by mass, carbon. Using $\approx$ 0.3 pg as the typical *E. coli*
89 dry mass (BNID: 103904, *Milo et al.* (*2010*)), we estimate that $\approx 10^{10}$ carbon atoms must be brought
90 into the cell in order to double all of the carbon-containing molecules (*Figure 2*(A, top))). Typical
91 laboratory growth conditions, such as those explored in the aforementioned proteomic data sets,
92 provide carbon as single class of sugar such as glucose, galactose, or xylose to name a few. *E.*
93 *coli* has evolved myriad mechanisms by which these sugars can be transported across the cell
94 membrane. One such mechanism of transport is via the PTS system which is a highly modular
95 system capable of transporting a diverse range of sugars (*Escalante et al., 2012*). The glucose-
96 specific component of this system transports $\approx$ 200 glucose molecules per second per channel
97 (BNID: 114686, *Milo et al.* (*2010*)). Making the assumption that this is a typical sugar transport rate,
98 coupled with the need to transport 10^{10} carbon atoms, we arrive at the conclusion that on the order
99 of 1,000 transporters must be expressed in order to bring in enough carbon atoms to divide in
100 6,000 s, diagrammed in the top panel of *Figure 2*(A). This estimate, along with the observed average
101 number of carbohydrate transporters present in the proteomic data sets (*Schmidt et al., 2016*;
102 *Peebo et al., 2015*; *Valgepea et al., 2013*; *Li et al., 2014*), is shown in *Figure 2*(A). While we estimate
103 1,000 transporters are needed, the data reveals that at a division time of $\approx 6,000$ s there is nearly
104 a ten-fold excess of transporters. Furthermore, the data illustrates that the average number of
105 carbohydrate transporters present is largely-growth rate independent.

106 The estimate presented in *Figure 2*(A) neglects any specifics of the regulation of carbon transport
107 system and presents a data-averaged view of how many carbohydrate transporters are present
108 on average. Using the diverse array of growth conditions explored in the proteomic data sets, we
109 can explore how individual carbon transport systems depend on the population growth rate. In
110 *Figure 2*(B), we show the total number of carbohydrate transporters specific to different carbon
111 sources. A striking observation, shown in the top-left plot of *Figure 2*(B), is the constancy in the
112 expression of the glucose-specific transport systems (the PtsG enzyme of the PTS system and the
113 glucose-transporting ManXYZ complex). Additionally, we note that the total number of glucose-
114 specific transporters is tightly distributed $\approx 10^4$ per cell, an order of magnitude beyond the estimate
115 shown in *Figure 2*(A). This illustrates that *E. coli* maintains a substantial number of complexes
116 present for transporting glucose which is known to be the preferential carbon source (*Monod, 1947*;
117 *Liu et al., 2005*; *Aidelberg et al., 2014*).

118 It is now understood that a large number of metabolic operons are regulated with dual-input
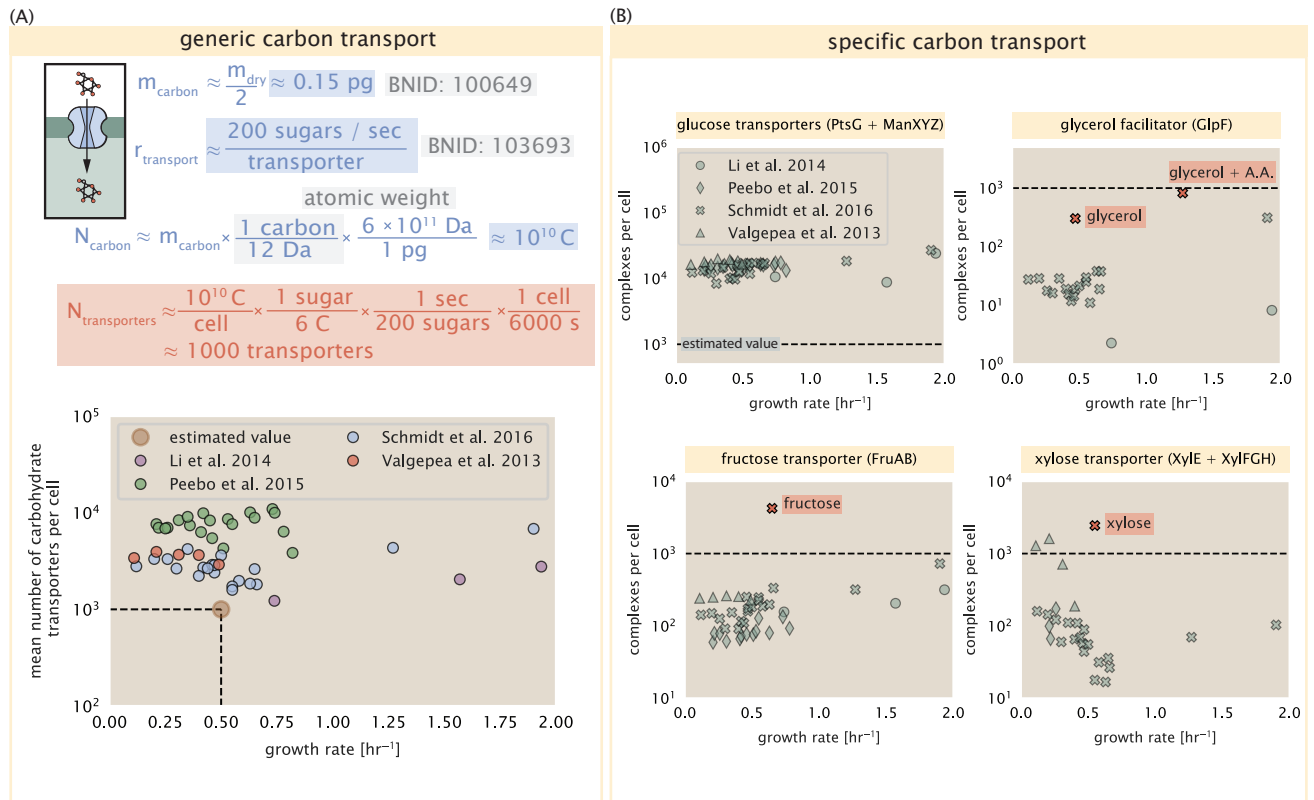
Figure 2. The abundance of carbon transport systems across growth rates. (A) A simple estimate for the minimum number of generic carbohydrate transport systems (top) assumes $\approx 10^{10}$ C are needed to complete division, each transported sugar contains ≈ 6 C, and each transporter conducts sugar molecules at a rate of ≈ 200 per second. Bottom plot shows the estimated number of transporters needed at a growth rate of ≈ 0.5 per hr (light-brown point and dashed lines). Colored points correspond to the mean number of carbohydrate transporters for different growth conditions across different published datasets. (B) The abundance of various specific carbon transport systems plotted as a function of the population growth rate. Red points and red-highlighted text indicate conditions in which the only source of carbon in the growth medium induces expression of the transport system.

119 logic gates that are only expressed when glucose concentrations are low (mediated by cyclic-AMP
120 receptor protein CRP) and the concentration of other carbon sources are elevated (*Gama-Castro*
121 *et al., 2016*; *Zhang et al., 2014b*). A famed example of such dual-input regulatory logic is in the
122 regulation of the *lac* operon which is only natively activated in the absence of glucose and the
123 presence of allolactose, an intermediate in lactose metabolism (*Jacob and Monod, 1961*), though we
124 now know of many other such examples (*Ireland et al., 2020*; *Gama-Castro et al., 2016*; *Belliveau*
125 *et al., 2018*). This illustrates that once glucose is depleted from the environment, cells have a means
126 to dramatically increase the abundance of the specific transporter needed to digest the next sugar
127 that is present. Several examples of induced expression of a specific carbon-source transporters
128 are shown in *Figure 2*(B). Points colored in red (labeled by red text-boxes) correspond to growth
129 conditions in which the specific carbon source (glycerol, xylose, or fructose) is present. These
130 plots show that, in the absence of the particular carbon source, expression of the transporters is
131 maintained on the order of $\sim 10^2$ per cell. However, when induced, the transporters become highly-
132 expressed and are present on the order of $\sim 10^4$ per cell, which exceeds the generic estimate given
133 in *Figure 2*(A). Together, this generic estimation and the specific examples of induced expression
134 suggest that transport of carbon across the cell membrane, while critical for growth, is not the
135 rate-limiting step of cell division.

136 In the context of speeding up growth, one additional limitation is the fact that the cell's inner
137 membrane is occupied by a multitude of other membrane proteins. Considering a rule-of-thumb
138 for the surface area of *E. coli* of about 6 μm^2 (BNID: 101792, *Milo et al.* (*2010*)), we expect an
139 areal density for 1,000 transporters to be approximately 200 transporters/μm^2. For a glucose
140 transporter occupying about 50 nm^2/dimer, this amounts to about only 1 percent of the total inner
141 membrane (*Szenk et al., 2017*). In addition, bacterial cell membranes typically have densities of
142 10^5 proteins//μm^2 (*Phillips, 2018*), implying that the cell could accommodate more transporters if it
143 were rate limiting.

Phosphorus and Sulfur Transport

145 We now turn our attention towards other essential elements, namely phosphorus and sulfur.
146 Phosphorus is critical to the cellular energy economy in the form of high-energy phosphodiester
147 bonds making up DNA, RNA, and the NTP energy pool as well as playing a critical role in the post-
148 translational modification of proteins and defining the polar-heads of lipids. In total, phosphorus
149 makes up ≈3% of the cellular dry mass which in typical experimental conditions is in the form of
150 inorganic phosphate. The cell membrane has remarkably low permeability to this highly-charged
151 and critical molecule, therefore requiring the expression of active transport systems. In *E. coli*, the
152 proton electrochemical gradient across the inner membrane is leveraged to transport inorganic
153 phosphate into the cell (*Rosenberg et al., 1977*). Proton-solute symporters are widespread in *E. coli*
154 (*Ramos and Kaback, 1977*; *Booth et al., 1979*) and can have rapid transport rates of 50 molecules
155 per second for sugars and other solutes (BNID: 103159; 111777, *Milo et al.* (*2010*)). In *E. coli* the PitA
156 phosphate transport system has been shown to very tightly coupled with the proton electrochemical
157 gradient with a 1:1 proton:phosphate stoichiometric ratio (*Harris et al., 2001*; *Feist et al., 2007*).
158 Illustrated in *Figure 3*(A), we can estimate that ≈ 300 phosphate transporters are necessary to
159 maintain an ≈ 3% dry mass with a 6,000 s division time. This estimate is again satisfied when we
160 examine the observed copy numbers of PitA in proteomic data sets (plot in *Figure 3*(A)). While our
161 estimate is very much in line with the observed numbers, we emphasize that this is likely a slight
162 over estimate of the number of transporters needed as there are other phosphorous scavenging
163 systems, such as the ATP-dependent phosphate transporter Pst system which we have neglected.

164 Satisfied that there are a sufficient number of phosphate transporters present in the cell, we
165 now turn sulfur transport as another potentially rate limiting process. Similar to phosphate, sulfate
166 is highly-charged and not particularly membrane permeable, requiring active transport. While
167 there exists a H+/sulfate symporter in *E. coli*, it is in relatively low abundance and is not well
168 characterized (*Zhang et al., 2014a*). Sulfate is predominantly acquired via the ATP-dependent ABC

(A)

(B)
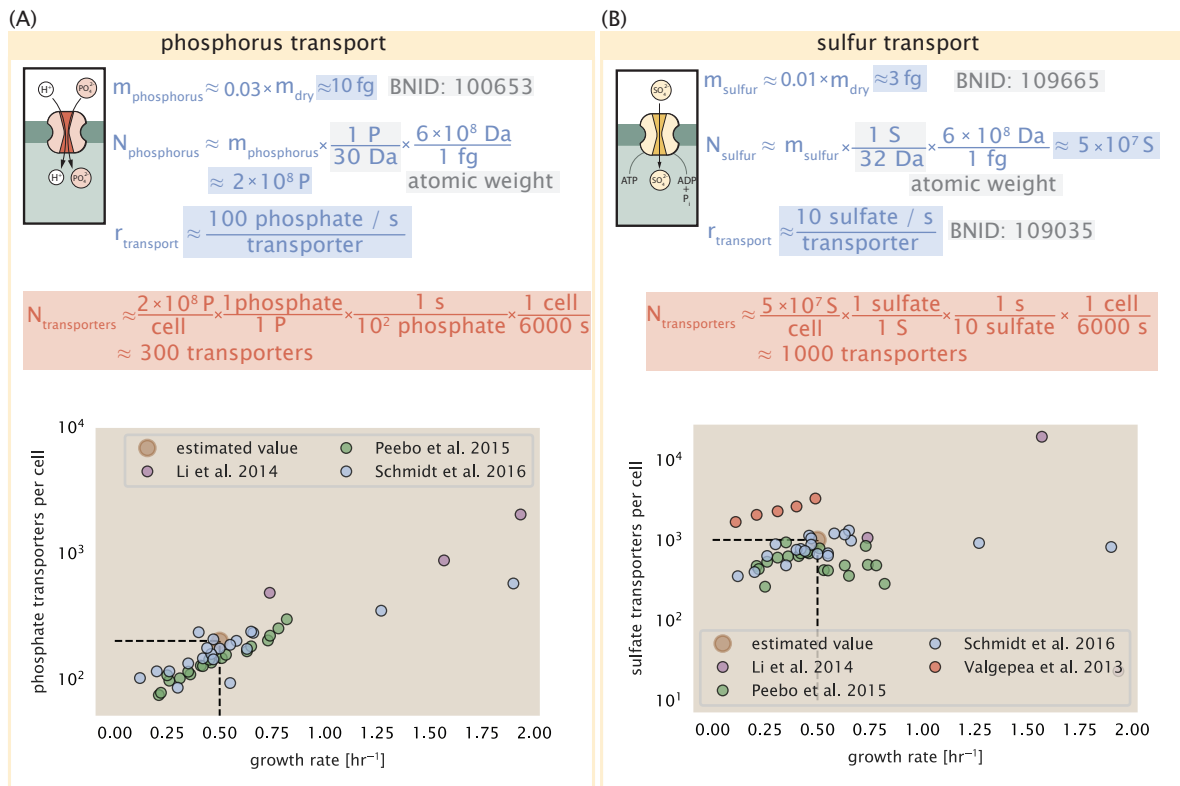
Figure 3. Estimates and measurements of phosphate and sulfate transport systems as a function of growth rate. (A) Estimate for the number of PitA phosphate transport systems needed to maintain a 3% phosphorus *E. coli* dry mass. Points in plot correspond to the the total number of PitA transporters per cell. (B) Estimate of the number of CysUWA complexes necessary to maintain a 1% sulfur *E. coli* dry mass. Points in plot correspond to average number of CysUWA transporter complexes that can be formed given the transporter stoichiometry [CysA]$_2$[CysU][CysW][Sbp/CysP].

169 transporter CysUWA system which also plays an important role in selenium transport (***Sekowska***
170 ***et al., 2000***; ***Sirko et al., 1995***). While specific kinetic details of this transport system are not readily
171 available, generic ATP transport systems in prokaryotes are on the order of 1 to 10 molecules per
172 second (BNID: 109035, ***Milo et al.*** (***2010***)). Combining this generic transport rate, measurement
173 of sulfur comprising 1% of dry mass, and a 6,000 second division time yields an estimate of $\approx$
174 1000 CysUWA complexes per cell (***Figure 3***(B)). Once again, this estimate is in notable agreement
175 with proteomic data sets, suggesting that there are sufficient transporters present to acquire the
176 necessary sulfur. In a similar spirit of our estimate of phosphorus transport, we emphasize that
177 this is likely an overestimate of the number of necessary transporters as we have neglected other
178 sulfur scavenging systems that are in lower abundance.

Nitrogen Transport

180 Finally, we turn to nitrogen transport as the last remaining transport system highlighted in ***Figure 1***.
181 Unlike phosphate, sulfate, and various sugar molecules, nitrogen in the form of ammonia can readily
182 diffuse across the cell membrane and has a permeability on par with water ($\approx 10^5$ nm/s, BNID:110824
183 ***Milo et al.*** (***2010***)). In particularly nitrogen-poor conditions, *E. coli* expresses a transporter (AmtB)
184 which appears to aid in nitrogen assimilation, though the mechanism and kinetic details of transport
185 is still a matter of debate (***van Heeswijk et al., 2013***; ***Khademi et al., 2004***). Beyond ammonia,
186 another plentiful source of nitrogen come in the form of glutamate, which has it's own complex
187 metabolism and scavenging pathways. However, nitrogen is plentiful in the growth conditions
188 examined in this work, permitting us to neglect nitrogen transport as a potential rate limiting
189 process in cell division.

Energy Production

While the transport of nutrients is required to build new cell mass, the metabolic pathways involved in assimilation both consumes and generates energy in the form of NTPs. The high-energy phosophodiester bonds of (primarily) ATP power a variety of cellular processes that drive biological systems away from thermodynamic equilibrium. Our next class of estimates consider the energy budget of a dividing cell in terms of the synthesis of ATP from ADP and inorganic phosphate as well as maintenance of the electrochemical proton gradient which powers it.

ATP Synthesis

Hydrolysis of the terminal phosphodiester bond of ATP forming ADP and an inorganic phosphate is a kinetic driving force in a wide array of biochemical reactions. One such reaction is the formation of peptide bonds during translation which requires ≈ 2 ATPs for the charging of an amino acid to the tRNA and ≈ 2 ATP equivalents for the formation of the peptide bond between amino acids. Together, these energetic costs consume $\approx 80\%$ of the cells ATP budget (BNID: 107782; 106158; 101637; 111918, *Milo et al.* (*2010*)). The pool of ATP is produced by the F_1-F_O ATP synthase – a membrane-bound rotary motor which under ideal conditions can yield ≈ 300 ATP per second (BNID: 114701; *Milo et al.* (*2010*); *Weber and Senior* (*2003*)).
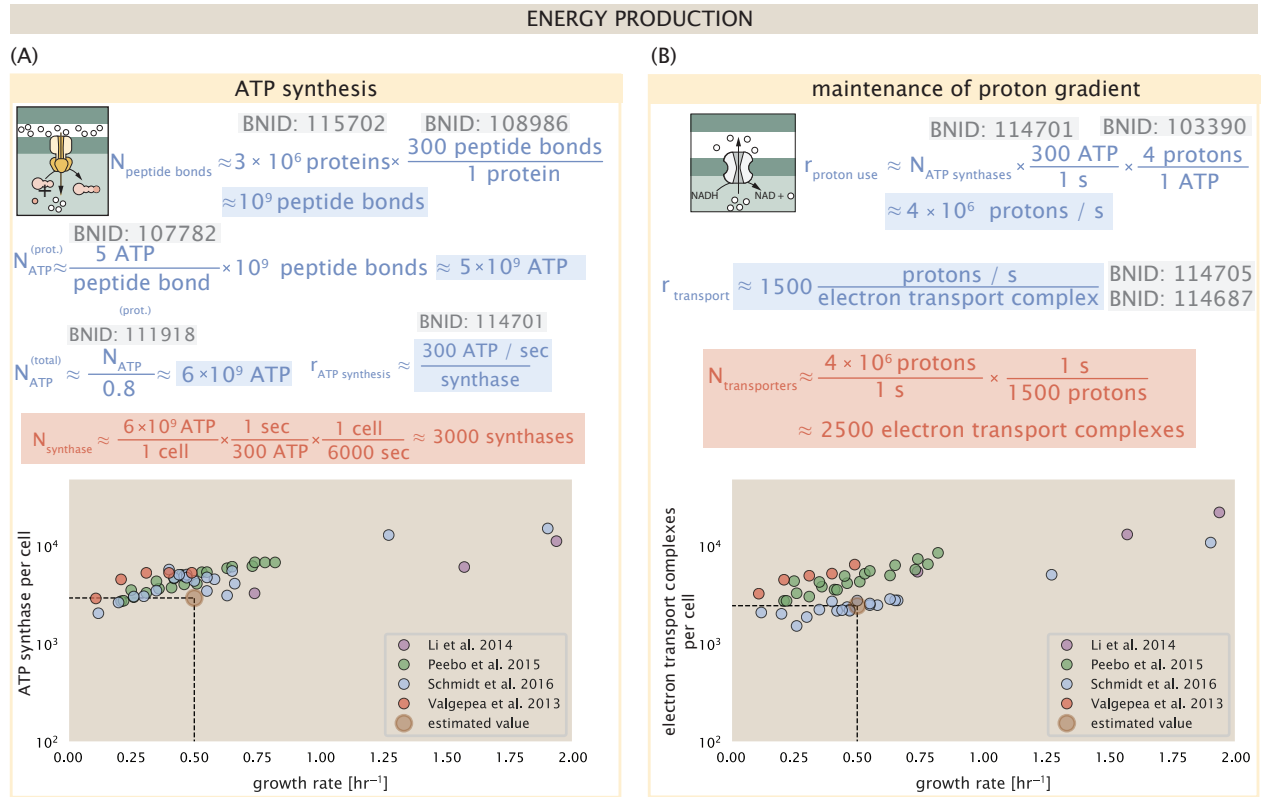
To estimate the total number of ATP equivalents consumed during a cell cycle, we will make the approximation that there are $\approx 3 \times 10^6$ proteins per cell with an average protein length of $\approx$ 300 peptide bonds (BNID: 115702; 108986; 104877, *Milo et al.* (*2010*)). Together, we arrive at the estimate that the typical *E. coli* cell consumes $\approx 5 \times 10^9$ ATP per cell cycle on protein synthesis alone and $\approx 6 \times 10^9$ ATP in total. Assuming that the ATP synthases are operating at their fastest possible rate, we arrive at an estimate that ≈ 3000 ATP synthases are needed to keep up with the energy demands of the cell. This estimate and a comparison with the data are shown in *Figure 4*(A). Despite our assumption of maximal ATP production rate per synthase and approximation of all NTP consuming reactions being the same as ATP, we find that an estimate of a few thousand complete synthases per cell to agree well with the experimental data.

Generating the Proton Electrochemical Gradient

In order to produce ATP, the F_1-F_O ATP synthase itself must consume energy. Rather than burning through its own product, this intricate macromolecular machine has evolved to exploit the electrochemical potential established across the inner membrane through cellular respiration. This electrochemical gradient is manifest by the pumping of protons into the intermembrane space via the electron transport chains as they reduce NADH. In *E. coli*, this potential difference is ≈ -200 mV (BNID: 102120, *Milo et al.* (*2010*)). As estimated in the supporting information, this potential difference is generated by maintaining $\approx 2 \times 10^4$ protons in the intermembrane space.

However, the constant rotation of the ATP synthases would rapidly abolish this potential difference if it were not being actively maintained. To undergo a complete rotation (and produce a single ATP), the F_1-F_O ATP synthase must shuttle ≈ 4 protons across the membrane into the cytosol (BNID: 103390, *Milo et al.* (*2010*)). With ≈ 3000 ATP synthases each generating 300 ATP per second, the 2×10^4 protons establishing the 200 mV potential would consumed in only a few milliseconds! This brings us to our next estimate: how many electron transport complexes are needed to support the consumption rate of the ATP synthases?

The electrochemistry of the electron transport complexes of *E. coli* have been the subject of intense biochemical and biophysical study over the past half century (*Ingledew and Poole, 1984*; *Khademian and Imlay, 2017*; *Cox et al., 1970*; *Henkel et al., 2014*). A recent work (*Szenk et al., 2017*) examined the respiratory capacity of the *E. coli* electron transport complexes using structural and biochemical data, revealing that each electron transport chain rapidly pumps protons into the intermembrane space at a clip of ≈ 5000 protons per second (BIND: 114704; 114687, *Milo et al.* (*2010*)). Using our estimate of the number of ATP synthases required per cell (*Figure 4*(A)), coupled with these recent measurements, we estimate that ≈ 1000 electron transport complexes would be

ENERGY PRODUCTION

(A)

ATP synthesis

BNID: 115702   BNID: 108986

$$N_{peptide\ bonds} \approx 3 \times 10^6\ proteins \times \frac{300\ peptide\ bonds}{1\ protein}$$

$$\approx 10^9\ peptide\ bonds$$

BNID: 107782

$$N_{ATP}^{(prot.)} \approx \frac{5\ ATP}{peptide\ bond} \times 10^9\ peptide\ bonds \approx 5 \times 10^9\ ATP$$

BNID: 111918

$$N_{ATP}^{(total)} \approx \frac{N_{ATP}^{(prot.)}}{0.8} \approx 6 \times 10^9\ ATP \qquad r_{ATP\ synthesis} \approx \frac{300\ ATP\ /\ sec}{synthase}$$

BNID: 114701

$$N_{synthase} \approx \frac{6 \times 10^9\ ATP}{1\ cell} \times \frac{1\ sec}{300\ ATP} \times \frac{1\ cell}{6000\ sec} \approx 3000\ synthases$$

(B)

maintenance of proton gradient

BNID: 114701   BNID: 103390

$$r_{proton\ use} \approx N_{ATP\ synthases} \times \frac{300\ ATP}{1\ s} \times \frac{4\ protons}{1\ ATP}$$

$$\approx 4 \times 10^6\ protons\ /\ s$$

$$r_{transport} \approx 1500\ \frac{protons\ /\ s}{electron\ transport\ complex} \quad \begin{array}{l} BNID:\ 114705 \\ BNID:\ 114687 \end{array}$$

$$N_{transporters} \approx \frac{4 \times 10^6\ protons}{1\ s} \times \frac{1\ s}{1500\ protons}$$

$$\approx 2500\ electron\ transport\ complexes$$

Figure 4. The abundance of F_1-F_O ATP synthases and electron transport chain complexes as a function of growth rate. (A) Estimate of the number of F_1-F_O ATP synthase complexes needed accommodate peptide bond formation and other NTP dependent processes Points in plot at bottom correspond to the mean number of complete F_1-F_O ATP synthase complexes that can be formed given proteomic measurements and the subunit stoichiometry $[AtpE]_{10}[AtpF]_2[AtpB][AtpC][AtpH][AtpA]_3[AtpG][AtpD]_3$. (B) Estimate of the number of electron transport chain complexes needed to maintain a membrane potential of −200 mV given estimate of number of F_1-F_O ATP synthases from (A). Points in plot correspond to the average number of complexes identified as being involed in aerobic respiratoion by the Gene Ontology identifier GO:0019646 that could be formed given proteomic observations. These complexes include cytochromes *bd1* ([CydA][CydB][CydX][CydH]), *bdII* ([AppC][AppB]), *bo3*,([CyoD][CyoA][CyoB][CyoC]) and NADH:quinone oxioreducase I ([NuoA][NuoH][NuoJ][NuoK][NuoL][NuoM][NuoN][NuoB][NuoC][NuoE][NuoF][NuoG][NuoI]) and II ([Ndh]).

239 necessary to facilitate the $\approx 4 \times 10^6$ protons per second diet of the celllular ATP synthases. This
240 estimate is in agreement with the number of complexes identified in the proteomic datasets (plot
241 in *Figure 4*(B)).

242 **Energy production in a crowded membrane.**
243 For each protein considered so far, the data shows that in general their numbers increase with
244 growth rate. This is in part a consequence of the increase in cell length and width at that is common
245 to many rod-shaped bacteria at faster growth rates (*Ojkic et al., 2019*; *Harris and Theriot, 2018*).
246 For the particular case of *E. coli*, the total cellular protein and cell size increase logarithmically
247 with growth rate (*Schaechter et al., 1958*; *Si et al., 2017*). Indeed, this is one reason why we have
248 considered only a single, common growth condition across all our estimates so far. Such a scaling
249 will require that the total number of proteins and net demand on resources also grow in proportion
250 to the increase in cell size divided by the cell's doubling time. Recall however that each transport
251 process, as well as the ATP production via respiration, is performed at the bacterial membrane. This
252 means that their maximum productivity can only increase in proportion to the cell's surface area
253 divided by the cell doubling time. This difference in scaling would vary in proportion to the surface
254 area-to-volume (S/V) ratio.
255   While we found that there was more than sufficient membrane real estate for carbon intake in

our earlier estimate, the total number of ATP synthases and electron chain transport complexes both exhibit a clear increase in copy number with growth rate, reaching in excess of 10^4 copies per cell (*Figure 4*). Here we consider the consequences of this S/V ratio scaling in more detail.

In our estimate of ATP production above we found that a cell demands about 6×10^9 ATP or 10^6 ATP/s. With a cell volume of roughly 1 fl, this corresponds to about 20 billion ATP per fl of cell volume, in line with previous estimates (*Stouthamer and Bettenhaussen, 1977*; *Szenk et al., 2017*). In *Figure 5*A we plot this ATP demand as a function of the S/V ratio in green, where we have considered a range of cell shapes from spherical to rod-shaped with an aspect ratio (length/width) equal to 4 (See appendix for calculations of cell volume and surface area). In order to consider the maximum power that could be produced, we consider the amount of ATP that can generated by a membrane filled with ATP synthase and electron transport complexes, which provides a maximal production of about 3 ATP / ($nm^2 \cdot s$) (*Szenk et al., 2017*). This is shown in red in *Figure 5*A, which shows that at least for the growth rates observed, the energy demand is roughly an order of magnitude less. For a rod-shaped bacterium like *E. coli*, the cell volume where demand would exceed the maximum energy production would correspond to a cell volume of about X fl. Interestingly, Szenk *et al.* also found that ATP production by respiration is less efficient than by fermentation per membrane area occupied due to the additional proteins of the electron transport chain. This suggests that even under anaerobic growth, there will be sufficient membrane space for ATP production in general.

While this serves to highlight the diminishing capacity to provide resources to grow if the cell increases in size (and its S/V decreases), the blue region in *Figure 5*(A) represents a somewhat unachievable limit since the inner membrane must also include other proteins such as those required for lipid and membrane synthesis. To gain some insight into this, we used the proteomic data to look at the distribution of proteins on the inner membrane. Here we use Gene Ontology (GO) annotations (*Ashburner et al., 2000*; *The Gene Ontology Consortium, 2018*) to identify all proteins embedded or peripheral to the inner membrane (GO term: 0005886). Those associated but not membrane-bound include proteins like MreB and ftsZ, that traverse the inner membrane by treadmilling and must nonetheless be considered as a vital component occupying space on the membrane. In *Figure 5*(B) we find that the total protein mass per μm is relatively constant with growth rate. Interestingly, when we consider the distribution of proteins grouped by their Clusters of Orthologous Groups (COG) (*Tatusov et al., 2000*), we find that relative abundance for those in metabolism (including ATP synthesis via respiration) is also relatively constant.

## Synthesis of the Cell Wall and lipid membrane.

[To be completed.]

Function of the Central Dogma

Up to this point, we have considered a variety of transport and biosynthetic processes that are critical to acquiring and generating new cell mass. While there are of course many other metabolic processes we could consider and perform estimates of (such as the components of fermentative versus aerobic respiration), we now turn our focus to some of the most central processes which *must* be undertaken irrespective of the growth conditions – the processes of the central dogma.

DNA

Most bacteria (including *E. coli*) harbor a single, circular chromosome and can have extra-chromosomal plasmids $\sim$ 100 kbp in length. We will focus our quantitative thinking solely on the chromosome of *E. coli* which harbors ≈ 5000 genes and $\approx 5 \times 10^6$ base pairs. To successfully divide and produce viable progeny, this chromosome must be faithfully replicated and segregated into each nascent cell. We again rely on the near century of literature in molecular biology to provide some insight towards the rates and mechanics of the replicative feat as well as the production of the replication starting materials, dNTPs.
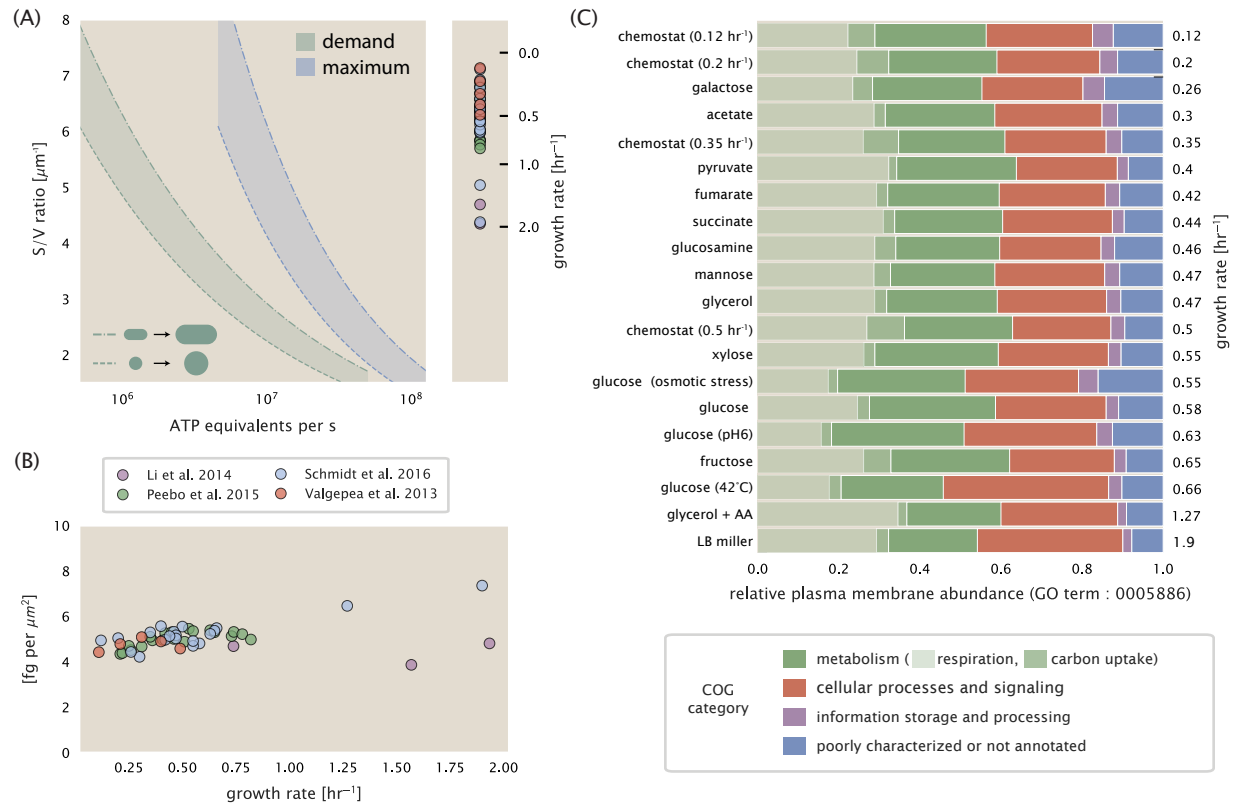
Figure 5. Influence of cell size and S/V ratio on ATP production and inner membrane composition. (A) Scaling of ATP demand and maximum ATP production as a function of S/V ratio. Cell volumes of 0.5 fl to X fl were considered, with the dash line corresponding to a cell with spherical shape, which the dash-dot line reflects a rod-shaped bacterium like *E. coli* with aspect ratio of 4. 50% of the bacterial inner membrane is assumed to be protein, with the remainder as lipid. (B) Total protein mass calculated for proteins with inner membrane annotation (GO term: 0005886). (C) Relative protein abundances by mass based on COG annotation. Metabolic proteins are further separated into respiration (F_1-F_O ATP synthase, NADH dehydrogenase I, succinate:quinone oxidoreductase, cytochrome bo_3 ubiquinol oxidase, cytochrome bd-I ubiquinol oxidase) and carbohydrate transport (GO term: GO:0008643). Note that the elongation factor EF-Tu can also associate with the inner membrane, but was excluded in this analysis due to its high relative abundance (roughly identical to the total mass shown in part (B)).

dNTP synthesis

We begin our exploration of the DNA replicative processes by examining the production of the deoxyribonucleotide triphosphates (dNTPs). The four major dNTPS (dATP, dTTP, dCTP, and dGTP) are synthesized *de novo* in separate pathways, requiring different building blocks. However, a critical step present in all dNTP synthesis pathways is the conversion from ribonucleotide to deoxyribonucleotide via the removal of the 3' hydroxyl group of the ribose ring CITE. This reaction is mediated by a class of enzymes termed ribonucleotide reductases, of which *E. coli* possesses two aerobically active complexes (termed I and II) and a single anaerobically active enzyme CITE. Due to their peculiar formation of a peculiar radical intermediate, these enzymes have received much biochemical kinetic and structural characterization. One such work (*Ge et al., 2003*) performed a detailed *in vitro* measurement of the steady-state kinetic rates of these complexes, revealing a turnover rate of ≈ 10 per second.

Considering this reaction (mediated by the ribonucleotide reductase complexes I and II) is central to synthesis of all dNTPS, it is reasonable to consider the abundance of these complexes as a measure of the total dNTP production in *E. coli*. Illustrated schematically in **??**(A), we consider the fact that to replicate the cell's genome, on the order of $\approx 10^7$ dNTPs must be synthesized. Assuming a production rate of 10 per second per ribonucleotide reductase complex and a cell division time of 6000 seconds, we arrive at an estimate of ≈ 150 complexes are needed per cell. As shown in the bottom panel of **??**(A), this estimate agrees with the experimental measurements of these complexes abundances within $\approx 1/2$ an order of magnitude.

Recent work has that during replication, the ribonucleotide reductases complexes localize into discrete foci colocalized with the DNA replisome complex (*Sánchez-Romero et al., 2011*). This is particularly pronounced in environments where growth is slow, indicating that spatial organization and regulation of the activity of the complexes plays an important role.

DNA Replication

We now turn our focus twoards the process of integration of the dNTP building blocks into the replicated chromosme strand via the DNA polymerase enzymes. Replication of bacterial chromosomes is initiated at a single region of the chromosome termed the *oriC* locus at which a pair of DNA polymerases bind and begin their high-fidelity replication of the genome in opposite directions. Assuming equivalence between the two replication forks, this means that the two DNA polymerases meet at the midway point of the circular chromosome termed the *ter* locus. This division of labor means The kinetics of the four types of DNA polymerases (I – V) have been intensely studied, revealing that DNA polymerase III performs the high fidelity processive replication of the genome with the other "accessory" polymerases playing auxiliary roles *Fijalkowska et al.* (*2012*). *In vitro* measurements have shown that DNA Polymerase III copies DNA at a rate of ≈ 600 nucleotides per second (BNID: 104120, *Milo et al.* (*2010*)). Thus, to replicate a single chromosome, two DNA polymerases replicating at their maximal rate would copy the entire genome in ≈ 4000 s. Thus, with a division time of 6000 s (our "typical" growth rate for the purposes of this work), there is sufficient time for a pair of DNA polymerases to replicate the entire genome. However, this estimate implies that 4000 s would be the upper-limit time scale for bacterial division which is at odds with the familiar ≈ 1500 s doubling time of *E. coli* in rich medium.

It is know well known that *E. coli* can parallelize its DNA replication such that multiple chromosomes are being replicated at once. Recent work (*Si et al., 2017*) has shown that the replicative timescale of cell division can be massively parallelized where *E. coli* can have on the order of 10 - 12 replication forks at a given time. Thus, even in rapidly growing cultures, only a few polymerases (≈ 10) are needed to replicate the chromosome. However, as shown in **??**(A), DNA polymerase III is nearly an nearly an order of magnitude more abundant. This discrepancy can be understood when considering the binding affinities. [GC: ... need to think this out. This feels like I am going far afield of the actual message of the paper.]

Protein synthesis

Lastly, we turn our attention to the process of translation. So far in our various estimates there has been little to suggest any apparent limit to how fast a bacterium might divide under steady-state growth. Even in our examples of *E. coli* grown rapidly under different carbohydrate sources (*Figure 2*(B)), cells are able to utilize less preferred carbon sources by inducing the expression of additional membrane transporters and enzymes. [Maybe go into Hwa style resource allocation with references added]. In this respect, gross overexpression of a protein can lead to a reduction of the growth rate.

We can determine the translation-limited growth rate by noting that the total number of peptide bonds created as the cell doubles N_{aa} will be given by, $\tau \cdot r_t \cdot R$. Here, τ refers to the doubling time of the cell under steady-state growth, r_t is the maximum translation rate, and R is the average number of ribosomes in the cell. With the growth rate related to the cell doubling time by $\lambda = ln(2)/\tau$, we can write the translation-limited growth rate as,

$$\lambda_{\text{translation-limited}} = \frac{ln(2) \cdot r_t \cdot R}{N_{aa}}. \tag{1}$$

Alternatively, since N_{aa} is related to the total protein mass through the molecular weight of each protein, we can also consider the growth rate in terms of ribosomal mass fraction. This calculation in shown in *Figure 6*(A). This allows us to rewrite the growth rate as,
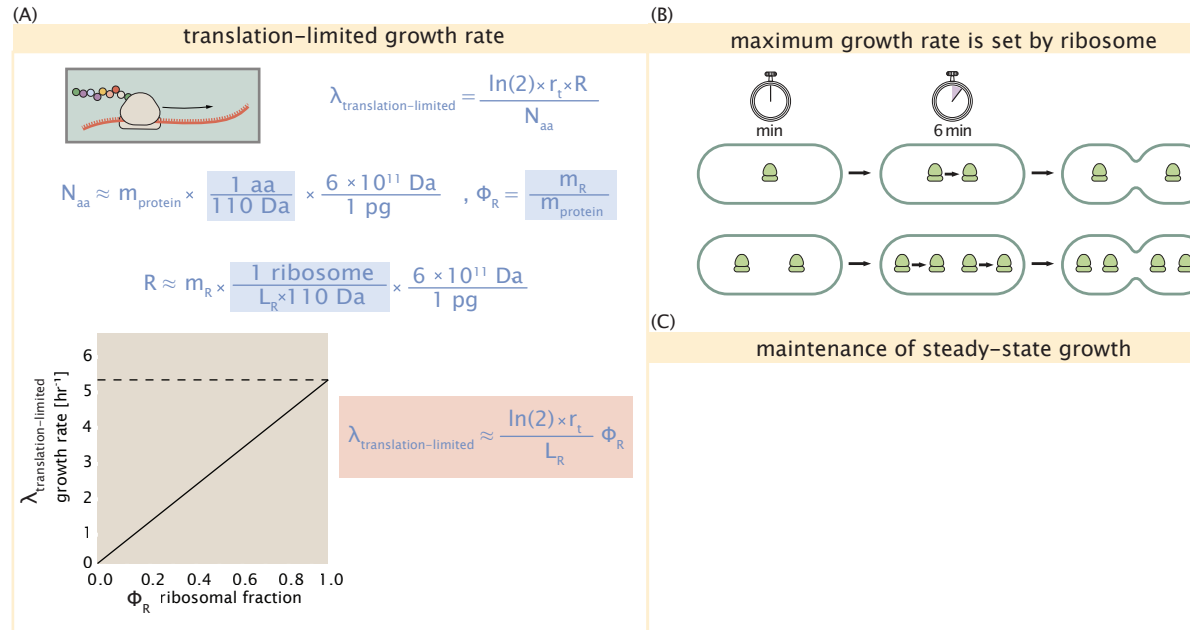
$$\lambda_{\text{translation-limited}} \approx \frac{ln(2) \cdot r_t}{L_R} \Phi_R, \tag{2}$$

where L_R is the total length in amino acids that make up a ribosome, and Φ_R is the ribosomal mass fraction. This is plotted as a function of ribosomal fraction Φ_R in *Figure 6*(A), with a translation rate $r_t = 17aa/s$ and $L_R =$[] aa, which corresponds to the length in amino acids for all ribosomal subunits of the 50S and 30S complexes and elongation factor required for translation.

Perhaps the first thing to notice is that there is a maximum growth rate at about $\lambda \approx 6hr^{-1}$, or doubling time of about 7 minutes. This maximum growth rate can be viewed as an inherent speed limit due to the need for the cell to double the cell's entire ribosomal mass. Interestingly, this limit is independent of the absolute number of ribosomes, but rather is simply given by time to translate an entire ribosome, L_R/r_t. As shown in *Figure 6*(B), we can reconcile this with the observation that in order to double the average number of ribosomes, each ribosome must produce a second ribosome. This is a process that cannot be parallelized further.

Since a cell consists of more than just ribosomes, we can see that for Φ_R in the range of about 0.1 - 0.3, the maximum growth rate is in line with experimentally reported growth rates around 0.5 - 2 hr^{-1}. Here we have implicitly assumed that translation proceeds randomly, without preference between ribosomal or non-ribosomal mRNA, which appears reasonable. Importantly, in order for a cell to scale this limit set by Φ_R the cell must increase it's ribosomal abundance, either by synthesizing more ribosomes or reducing the fraction of non-ribosomal proteins.

One additional point to note is that across different species of bacteria, cells do not decrease their ribosomal abundance to zero in the limit of poorer nutrient condition [CITE?]. Indeed, some organisms appear to have constant ribosomal abundance irrespective of their growth rate [NB: ask Griffin and figure out what organism this is]. From the perspective of a bacterium dealing with uncertain nutrient conditions, there is likely a benefit for the cell to maintain some relative fraction of ribosomes to support rapid growth as nutrient conditions improve. In addition, given their massive size at about 850 kDa, they may play an as-yet fully understood role as a crowding agent in cellular function *Delarue et al.* (*2018*); *Soler-Bistué et al.* (*2020*). If we consider a scenario where nutrient conditions become poorer and poorer, there must be a regime where the cell has more ribosomes than it can utilize. While this perhaps suggests less import to the process of translation, it is important to recognize that in order for a cell to maintain steady-state growth, the cell's translation capacity must be mitigated. Otherwise, ribosomes will deplete their supply of

(A)

translation–limited growth rate

$$\lambda_{\text{translation-limited}} = \frac{\ln(2) \times r_t \times R}{N_{aa}}$$

$$N_{aa} \approx m_{\text{protein}} \times \frac{1\ aa}{110\ Da} \times \frac{6 \times 10^{11}\ Da}{1\ pg} \quad , \quad \Phi_R = \frac{m_R}{m_{\text{protein}}}$$

$$R \approx m_R \times \frac{1\ \text{ribosome}}{L_R \times 110\ Da} \times \frac{6 \times 10^{11}\ Da}{1\ pg}$$

$$\lambda_{\text{translation-limited}} \approx \frac{\ln(2) \times r_t}{L_R}\ \Phi_R$$

(B)

maximum growth rate is set by ribosome

min   6 min

(C)

maintenance of steady–state growth

Figure 6. Translation-limited growth rate. (A) Here we consider the translation-limited growth as a function of ribosomal fraction. By mass balance, the time required to double the entire proteome ($N_{aa}/r_t\cdot$) sets the translation-limited growth rate, $\lambda_{\text{translation-limited}}$. Here N_{aa} is effectively the number of peptide bonds that must be translated, r_t is the translation elongation rate, and R is the number of ribosomes. This can also be re-written in terms of the ribosomal mass fraction $\Phi_R = m_R / m_{\text{protein}}$, where m_R is the total ribosomal mass and m_{protein} is the mass of all proteins in the cell. L_R refers to the summed length of the ribosome in amino acids. $\lambda_{\text{translation-limited}}$ is ploted as a function of Φ_R (solid line). (B) The dashed line in part (A) identifies a maximum growth rate that is set by the ribosome. Specifically, this growth rate corresponds to the time required to translation an entire ribosome, L_R/r_t . This is a result that is independent of the number of ribosomes in the cell as shown schematically here. (C)

Figure 7. . (A) (B) (C).

---

398 amino acids and this will bring translation and cell growth to a halt (*Figure 6*(C)). We will consider
399 the consequences of this in the case of *E. coli* next.

400 **Multiple replication forks provide one strategy to support faster growth.**
401 We now turn to our proteomic data from *E. coli* and plot the ribosomal fraction as a function of
402 reported growth rate. Here we find that the ribosomal fraction always increases with growth rate.
403 This is consistent with the behavior expected for *E. coli*, and an observation of intense study related
404 to the so-called nutrient-limited growth law. In terms of absolute ribosomal abundance, we find
405 that cells increase both their quantity and cellular concentration at faster growth.
406 One feature of *E. coli*, as well as other bacteria like *B. subtilis*, is the ability to begin replication of
407 multiple copies of its genome during a single cell cycle. This is achieved through multiple initiation
408 forks and nested DNA replication. [need to refer to work from to Jun lab here!! - under adder
409 mechanism, the cell appears to add a certain cell mass in proportion to its number of origins]. We
410 find that the ribosome copy number increases in proportion to the expected number of origins.
411 The process of nested DNA replication will lead to a bias in gene dosage for genes closer to the
412 origin of replication () Importantly, ribosomal protein and rRNA genes are closer to the origin of
413 replication *Scholz et al.* (*2019*) and this provides a natural way for *E. coli* to bias the proportion of
414 ribosomes at faster growth without the advent of additional gene regulation strategies. Given that
415 ribosomal genes in *E. coli* appear to be transcribed at their maximal rate at fast growth rates [cite??],
416 increasing ribosomal copy number through increased gene dosage represents a creative approach
417 for the cell to grow faster without gross down-regulation of non-ribosomal genes.

418 **References**
419 Aidelberg, G., Towbin, B. D., Rothschild, D., Dekel, E., Bren, A., and Alon, U. (2014). Hierarchy of non-glucose
420 sugars in Escherichia coli. *BMC Systems Biology*, 8(1):133.

421 Antonenko, Y. N., Pohl, P., and Denisov, G. A. (1997). Permeation of ammonia across bilayer lipid membranes
422 studied by ammonium ion selective microelectrodes. *Biophysical Journal*, 72(5):2187–2195.

423 Ashburner, M., Ball, C. A., Blake, J. A., Botstein, D., Butler, H., Cherry, J. M., Davis, A. P., Dolinski, K., Dwight,
424 S. S., Eppig, J. T., Harris, M. A., Hill, D. P., Issel-Tarver, L., Kasarskis, A., Lewis, S., Matese, J. C., Richardson, J. E.,
425 Ringwald, M., Rubin, G. M., and Sherlock, G. (2000). Gene Ontology: tool for the unification of biology. *Nature
426 Genetics*, 25(1):25–29.

427 Assentoft, M., Kaptan, S., Schneider, H.-P., Deitmer, J. W., de Groot, B. L., and MacAulay, N. (2016). Aquaporin 4
428 as a NH3 Channel. *Journal of Biological Chemistry*, 291(36):19184–19195.

429 Basan, M., Zhu, M., Dai, X., Warren, M., Sévin, D., Wang, Y.-P., and Hwa, T. (2015). Inflating bacterial cells by
430 increased protein synthesis. *Molecular Systems Biology*, 11(10):836.

431 Bauer, S. and Ziv, E. (1976). Dense growth of aerobic bacteria in a bench-scale fermentor. *Biotechnology and
432 Bioengineering*, 18(1):81–94. _eprint: https://onlinelibrary.wiley.com/doi/pdf/10.1002/bit.260180107.

433 Belliveau, N. M., Barnes, S. L., Ireland, W. T., Jones, D. L., Sweredoski, M. J., Moradian, A., Hess, S., Kinney, J. B., and
434 Phillips, R. (2018). Systematic approach for dissecting the molecular mechanisms of transcriptional regulation
435 in bacteria. *Proceedings of the National Academy of Sciences*, 115(21):E4796–E4805.

436 Booth, I. R., Mitchell, W. J., and Hamilton, W. A. (1979). Quantitative analysis of proton-linked transport systems.
437 The lactose permease of Escherichia coli. *Biochemical Journal*, 182(3):687–696.

438 Cox, G. B., Newton, N. A., Gibson, F., Snoswell, A. M., and Hamilton, J. A. (1970). The function of ubiquinone in
439 Escherichia coli. *Biochemical Journal*, 117(3):551–562.

Delarue, M., Brittingham, G. P., Pfeffer, S., Surovtsev, I. V., Pinglay, S., Kennedy, K. J., Schaffer, M., Gutierrez, J. I., Sang, D., Poterewicz, G., Chung, J. K., Plitzko, J. M., Groves, J. T., Jacobs-Wagner, C., Engel, B. D., and Holt, L. J. (2018). mTORC1 Controls Phase Separation and the Biophysical Properties of the Cytoplasm by Tuning Crowding. *Cell*, 174(2):338–349.e20.

Escalante, A., Salinas Cervantes, A., Gosset, G., and Bolívar, F. (2012). Current knowledge of the Escherichia coli phosphoenolpyruvate–carbohydrate phosphotransferase system: Peculiarities of regulation and impact on growth and product formation. *Applied Microbiology and Biotechnology*, 94(6):1483–1494.

Feist, A. M., Henry, C. S., Reed, J. L., Krummenacker, M., Joyce, A. R., Karp, P. D., Broadbelt, L. J., Hatzimanikatis, V., and Palsson, B. Ø. (2007). A genome-scale metabolic reconstruction for Escherichia coli K-12 MG1655 that accounts for 1260 ORFs and thermodynamic information. *Molecular Systems Biology*, 3(1):121.

Fijalkowska, I. J., Schaaper, R. M., and Jonczyk, P. (2012). DNA replication fidelity in Escherichia coli: A multi-DNA polymerase affair. *FEMS Microbiology Reviews*, 36(6):1105–1121.

Gama-Castro, S., Salgado, H., Santos-Zavaleta, A., Ledezma-Tejeida, D., Muñiz-Rascado, L., García-Sotelo, J. S., Alquicira-Hernández, K., Martínez-Flores, I., Pannier, L., Castro-Mondragón, J. A., Medina-Rivera, A., Solano-Lira, H., Bonavides-Martínez, C., Pérez-Rueda, E., Alquicira-Hernández, S., Porrón-Sotelo, L., López-Fuentes, A., Hernández-Koutoucheva, A., Moral-Chávez, V. D., Rinaldi, F., and Collado-Vides, J. (2016). RegulonDB version 9.0: High-level integration of gene regulation, coexpression, motif clustering and beyond. *Nucleic Acids Research*, 44(D1):D133–D143.

Ge, J., Yu, G., Ator, M. A., and Stubbe, J. (2003). Pre-Steady-State and Steady-State Kinetic Analysis of *E. coli* Class I Ribonucleotide Reductase. *Biochemistry*, 42(34):10071–10083.

Harris, L. K. and Theriot, J. A. (2018). Surface Area to Volume Ratio: A Natural Variable for Bacterial Morphogenesis. *Trends in microbiology*, 26(10):815–832.

Harris, R. M., Webb, D. C., Howitt, S. M., and Cox, G. B. (2001). Characterization of PitA and PitB from *Escherichia coli*. *Journal of Bacteriology*, 183(17):5008–5014.

Heldal, M., Norland, S., and Tumyr, O. (1985). X-ray microanalytic method for measurement of dry matter and elemental content of individual bacteria. *Applied and Environmental Microbiology*, 50(5):1251–1257.

Henkel, S. G., Beek, A. T., Steinsiek, S., Stagge, S., Bettenbrock, K., de Mattos, M. J. T., Sauter, T., Sawodny, O., and Ederer, M. (2014). Basic Regulatory Principles of Escherichia coli's Electron Transport Chain for Varying Oxygen Conditions. *PLoS ONE*, 9(9):e107640.

Hui, S., Silverman, J. M., Chen, S. S., Erickson, D. W., Basan, M., Wang, J., Hwa, T., and Williamson, J. R. (2015). Quantitative proteomic analysis reveals a simple strategy of global resource allocation in bacteria. *Molecular Systems Biology*, 11(2):e784–e784.

Ingledew, W. J. and Poole, R. K. (1984). The respiratory chains of Escherichia coli. *Microbiological Reviews*, 48(3):222–271.

Ireland, W. T., Beeler, S. M., Flores-Bautista, E., Belliveau, N. M., Sweredoski, M. J., Moradian, A., Kinney, J. B., and Phillips, R. (2020). Deciphering the regulatory genome of *Escherichia coli*, one hundred promoters at a time. *bioRxiv*.

Jacob, F. and Monod, J. (1961). Genetic regulatory mechanisms in the synthesis of proteins. *Journal of Molecular Biology*, 3(3):318–356.

Jun, S., Si, F., Pugatch, R., and Scott, M. (2018). Fundamental principles in bacterial physiology - history, recent progress, and the future with focus on cell size control: A review. *Reports on Progress in Physics*, 81(5):056601.

Khademi, S., O'Connell, J., Remis, J., Robles-Colmenares, Y., Miercke, L. J. W., and Stroud, R. M. (2004). Mechanism of Ammonia Transport by Amt/MEP/Rh: Structure of AmtB at 1.35 Å. *Science*, 305(5690):1587–1594.

Khademian, M. and Imlay, J. A. (2017). *Escherichia Coli* cytochrome *c* peroxidase is a respiratory oxidase that enables the use of hydrogen peroxide as a terminal electron acceptor. *Proceedings of the National Academy of Sciences*, 114(33):E6922–E6931.

Li, G.-W., Burkhardt, D., Gross, C., and Weissman, J. S. (2014). Quantifying absolute protein synthesis rates reveals principles underlying allocation of cellular resources. *Cell*, 157(3):624–635.

Liu, M., Durfee, T., Cabrera, J. E., Zhao, K., Jin, D. J., and Blattner, F. R. (2005). Global Transcriptional Programs Reveal a Carbon Source Foraging Strategy by *Escherichia coli*. *Journal of Biological Chemistry*, 280(16):15921–15927.

Milo, R., Jorgensen, P., Moran, U., Weber, G., and Springer, M. (2010). BioNumbers—the database of key numbers in molecular and cell biology. *Nucleic Acids Research*, 38(suppl_1):D750–D753.

Monod, J. (1947). The phenomenon of enzymatic adaptation and its bearings on problems of genetics and cellular differentiation. *Growth Symposium*, 9:223–289.

Neidhardt, F. C., Ingraham, J., and Schaechter, M. (1991). *Physiology of the Bacterial Cell - A Molecular Approach*, volume 1. Elsevier.

Ojkic, N., Serbanescu, D., and Banerjee, S. (2019). Surface-to-volume scaling and aspect ratio preservation in rod-shaped bacteria. *eLife*, 8:642.

Peebo, K., Valgepea, K., Maser, A., Nahku, R., Adamberg, K., and Vilu, R. (2015). Proteome reallocation in *Escherichia coli* with increasing specific growth rate. *Molecular BioSystems*, 11(4):1184–1193.

Phillips, R. (2018). Membranes by the Numbers. In *Physics of Biological Membranes*, pages 73–105. Springer, Cham, Cham.

Ramos, S. and Kaback, H. R. (1977). The relation between the electrochemical proton gradient and active transport in Escherichia coli membrane vesicles. *Biochemistry*, 16(5):854–859.

Rosenberg, H., Gerdes, R. G., and Chegwidden, K. (1977). Two systems for the uptake of phosphate in Escherichia coli. *Journal of Bacteriology*, 131(2):505–511.

Sánchez-Romero, M. A., Molina, F., and Jiménez-Sánchez, A. (2011). Organization of ribonucleoside diphosphate reductase during multifork chromosome replication in Escherichia coli. *Microbiology*, 157(8):2220–2225.

Schaechter, M., MaalØe, O., and Kjeldgaard, N. O. (1958). Dependency on Medium and Temperature of Cell Size and Chemical Composition during Balanced Growth of *Salmonella typhimurium*. *Microbiology*, 19(3):592–606.

Schmidt, A., Kochanowski, K., Vedelaar, S., Ahrné, E., Volkmer, B., Callipo, L., Knoops, K., Bauer, M., Aebersold, R., and Heinemann, M. (2016). The quantitative and condition-dependent *Escherichia coli* proteome. *Nature Biotechnology*, 34(1):104–110.

Scholz, S. A., Diao, R., Wolfe, M. B., Fivenson, E. M., Lin, X. N., and Freddolino, P. L. (2019). High-Resolution Mapping of the Escherichia coli Chromosome Reveals Positions of High and Low Transcription. *Cell Systems*, 8(3):212–225.e9.

Scott, M., Gunderson, C. W., Mateescu, E. M., Zhang, Z., and Hwa, T. (2010). Interdependence of cell growth and gene expression: origins and consequences. *Science*, 330(6007):1099–1102.

Sekowska, A., Kung, H.-F., and Danchin, A. (2000). Sulfur Metabolism in Escherichia coli and Related Bacteria: Facts and Fiction. *Journal of Molecular Microbiology and Biotechnology*, 2(2):34.

Si, F., Li, D., Cox, S. E., Sauls, J. T., Azizi, O., Sou, C., Schwartz, A. B., Erickstad, M. J., Jun, Y., Li, X., and Jun, S. (2017). Invariance of Initiation Mass and Predictability of Cell Size in Escherichia coli. *Current Biology*, 27(9):1278–1287.

Sirko, A., Zatyka, M., Sadowy, E., and Hulanicka, D. (1995). Sulfate and thiosulfate transport in Escherichia coli K-12: Evidence for a functional overlapping of sulfate- and thiosulfate-binding proteins. *Journal of Bacteriology*, 177(14):4134–4136.

Soler-Bistué, A., Aguilar-Pierlé, S., Garcia-Garcerá, M., Val, M.-E., Sismeiro, O., Varet, H., Sieira, R., Krin, E., Skovgaard, O., Comerci, D. J., Eduardo P. C. Rocha, and Mazel, D. (2020). Macromolecular crowding links ribosomal protein gene dosage to growth rate in Vibrio cholerae. *BMC Biology*, 18(1):1–18.

Stasi, R., Neves, H. I., and Spira, B. (2019). Phosphate uptake by the phosphonate transport system PhnCDE. *BMC Microbiology*, 19.

Stouthamer, A. H. and Bettenhaussen, C. W. (1977). A continuous culture study of an ATPase-negative mutant of Escherichia coli. *Archives of Microbiology*, 113(3):185–189.

Szenk, M., Dill, K. A., and de Graff, A. M. R. (2017). Why Do Fast-Growing Bacteria Enter Overflow Metabolism? Testing the Membrane Real Estate Hypothesis. *Cell Systems*, 5(2):95–104.

Tatusov, R. L., Galperin, M. Y., Natale, D. A., and Koonin, E. V. (2000). The COG database: a tool for genome-scale analysis of protein functions and evolution. *Nucleic Acids Research*, 28(1):33–36.

Taymaz-Nikerel, H., Borujeni, A. E., Verheijen, P. J. T., Heijnen, J. J., and van Gulik, W. M. (2010). Genome-derived minimal metabolic models for Escherichia coli MG1655 with estimated in vivo respiratory ATP stoichiometry. *Biotechnology and Bioengineering*, 107(2):369–381. _eprint: https://onlinelibrary.wiley.com/doi/pdf/10.1002/bit.22802.

The Gene Ontology Consortium (2018). The Gene Ontology Resource: 20 years and still GOing strong. *Nucleic Acids Research*, 47(D1):D330–D338.

Valgepea, K., Adamberg, K., Seiman, A., and Vilu, R. (2013). *Escherichia coli* achieves faster growth by increasing catalytic and translation rates of proteins. *Molecular BioSystems*, 9(9):2344.

van Heeswijk, W. C., Westerhoff, H. V., and Boogerd, F. C. (2013). Nitrogen Assimilation in *Escherichia coli*: Putting Molecular Data into a Systems Perspective. *Microbiology and Molecular Biology Reviews*, 77(4):628–695.

Weber, J. and Senior, A. E. (2003). ATP synthesis driven by proton transport in F1F0-ATP synthase. *FEBS Letters*, 545(1):61–70.

Willsky, G. R., Bennett, R. L., and Malamy, M. H. (1973). Inorganic Phosphate Transport in Escherichia coli: Involvement of Two Genes Which Play a Role in Alkaline Phosphatase Regulation. *Journal of Bacteriology*, 113(2):529–539.

Zhang, L., Jiang, W., Nan, J., Almqvist, J., and Huang, Y. (2014a). The Escherichia coli CysZ is a pH dependent sulfate transporter that can be inhibited by sulfite. *Biochimica et Biophysica Acta (BBA) - Biomembranes*, 1838(7):1809–1816.

Zhang, Z., Aboulwafa, M., and Saier, M. H. (2014b). Regulation of **crp** Gene Expression by the Catabolite Repressor/Activator, Cra, in **Escherichia coli**. *Journal of Molecular Microbiology and Biotechnology*, 24(3):135–141.